








Electrically driven transient and permanent phase transformations in highly strained epitaxial BiFeO₃ thin films ^{EP}

Cite as: APL Mater. **8**, 101110 (2020); <https://doi.org/10.1063/5.0025673>

Submitted: 17 August 2020 . Accepted: 06 October 2020 . Published Online: 20 October 2020

 Hyeon Jun Lee, Jeongyong Kim, Seung Hyun Hwang,  Hyeokmin Choe,  Semen Gorfman, Yeong-Jae Heo, Su Yong Lee,  Pierre-Eymeric Janolin, Igor Kornev, Tobias U. Schüllli, Carsten Richter, Joo-Hyoung Lee,  Ullrich Pietsch,  Chan-Ho Yang, and  Ji Young Jo

COLLECTIONS

 This paper was selected as an Editor's Pick



View Online



Export Citation



CrossMark

ARTICLES YOU MAY BE INTERESTED IN

[Anisotropic, meandering domain microstructure in the improper ferroelectric CsNbW₂O₉](#)

APL Materials **8**, 101108 (2020); <https://doi.org/10.1063/5.0026040>

[A new era in ferroelectrics](#)

APL Materials **8**, 120902 (2020); <https://doi.org/10.1063/5.0034914>

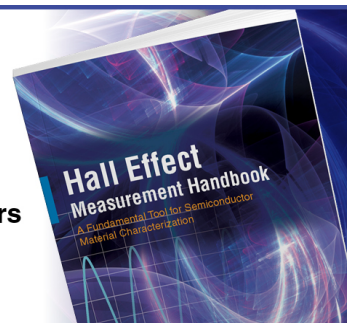
[Dynamic excitations of chiral magnetic textures](#)

APL Materials **8**, 100903 (2020); <https://doi.org/10.1063/5.0027042>

Hall Effect Measurement Handbook

A comprehensive resource for researchers

Explore theory, methods, sources of errors, and ways to minimize the effects of errors



Request it here

 Lake Shore
CRYOTRONICS

Electrically driven transient and permanent phase transformations in highly strained epitaxial BiFeO₃ thin films

Cite as: APL Mater. 8, 101110 (2020); doi: 10.1063/5.0025673

Submitted: 17 August 2020 • Accepted: 6 October 2020 •

Published Online: 20 October 2020



Hyeon Jun Lee,¹  Jeongyong Kim,² Seung Hyun Hwang,¹ Hyeokmin Choe,³  Semen Gorfman,⁴  Yeong-Jae Heo,¹ Su Yong Lee,⁵ Pierre-Eymeric Janolin,⁶  Igor Kornev,⁶ Tobias U. Schüllli,⁷ Carsten Richter,⁷ Joo-Hyoung Lee,¹ Ullrich Pietsch,⁸  Chan-Ho Yang,²  and Ji Young Jo^{1,a)} 

AFFILIATIONS

¹School of Materials Science and Engineering, Gwangju Institute of Science and Technology, Gwangju 61005, South Korea

²Department of Physics, Korea Advanced Institute of Science and Technology, Daejeon 34141, South Korea

³Materials Science and Engineering Division, National Institute of Standards and Technology, Gaithersburg, Maryland 20899, USA

⁴Department of Materials Science and Engineering, Tel Aviv University, Tel Aviv 6997801, Israel

⁵Pohang Accelerator Laboratory, Pohang University of Science and Technology, Pohang 37676, South Korea

⁶Université Paris-Saclay, CentraleSupélec, CNRS, Laboratoire SPMS, 91190 Gif-sur-Yvette, France

⁷ESRF-The European Synchrotron, 71 Avenue des Martyrs, 38043 Grenoble, France

⁸Department of Physics, University of Siegen Emmy-Noether-Campus, Walter-Flex-Str. 3, Siegen 57072, Germany

^{a)} Author to whom correspondence should be addressed: jjyo@gist.ac.kr

ABSTRACT

Electric-field-driven phase transformation phenomena in multiferroic BiFeO₃ are directly linked to the functionalities of electronic devices based on multiferroic materials. Understanding how the transformation evolves at the nanoscale under the influence of an electric field will provide fascinating insights into key parameters that utilize the transformation features. Here, we report both the electric-field-driven transient and permanent phase transformations in highly strained BiFeO₃ thin films and their transformation dynamics at the nanoscale. We found that two distinct transient and permanent phase transformations were triggered below and above a coercive voltage of the polymorphic phase, indicating that ferroelectric polarization switching could promote permanent phase transformations. We also found that the transient transformations evolve via complex phase boundary motions between the coexisting phases, whereas permanent transformations occurred via nucleation of the other phases.

© 2020 Author(s). All article content, except where otherwise noted, is licensed under a Creative Commons Attribution (CC BY) license (<http://creativecommons.org/licenses/by/4.0/>). <https://doi.org/10.1063/5.0025673>

I. INTRODUCTION

Phase transformation in a solid is the most effective method for controlling its electronic and/or structural functionalities, which can be utilized to tailor electronic devices. The recently developed nanoscale thin film deposition, such as epitaxial growth, has been used to form steady-state crystalline structures and modify their functionalities directly linked to the phases. For example, the epitaxial film growth of BiFeO₃ (BFO), which possesses ferroelectricity and

magnetism at the room temperature, can exhibit the phase transformation in association with a significant change in multiferroic order parameters.^{1–6} The epitaxial strain-dependence of energy landscape of BFO causes the irreversible phase transformation between the coexisting tetragonal (T) and polymorphic phase (S)—similar to the bulk rhombohedral phase in BFO.⁷ One feasible method to induce the phase transformation is by the application of an electric field.^{3,8,9} The magnitude of the applied electric field can be quantitatively related to the volume fractions of the T and S phases of BFO in

association with the transient phase transformation.⁹ An electric field above the threshold field can lead to a permanent phase transformation even after a removal of the electric field,^{10–12} which would be a novel route to manipulate the functionalities of multiferroic materials.

Ferroelectric polarization rotation and/or switching toward the direction in parallel with the electric field has been predicted to drive the permanent phase transformation.¹⁰ Recently, density functional theory (DFT) calculations revealed that the T phase of BFO (T-BFO) becomes energetically favorable when the lattice is expanded along the *out-of-plane* direction.^{13,14} Over the last decade, the experimental studies that investigate these transformations and their associated mechanisms have been reported.^{8,10,11,15,16} Predominantly several *ex situ* scanning probe microscopy studies have reported abrupt morphological changes of BFO before and after the application of an electric field as evidence for the permanent phase transformation.^{10,15} The role of the ferroelectric polarization direction in determining the threshold field is controversial due to the lack of information on the polarization state in each crystalline phase in the mixed area.^{8,11,16} In addition to the permanent phase transformation, the transient transformation, which occurs only when an electric field is applied, has been reported using *in situ* x-ray microdiffraction (X μ D) in the presence of an applied electric field.⁹ The transient phase transformation is accompanied with a larger variation in volume fraction compared to the permanent phase transformation. However, there are still crucial unaddressed questions regarding the feasible manipulation of phase transformations as well as the corresponding functionalities of multiferroic materials: (1) what are the key parameters that determine the transient and permanent phase transformations and (2) what is the threshold field for inducing the permanent phase transformation.⁷

Here, we report the nanoscale dynamics of electric-field-driven transient and permanent phase transformations in highly strained BFO thin films consisting of the multiple crystalline phases. The phase transformation of multiple crystalline phases has been quantitatively measured using *in situ* X μ D under an application of sequential electric pulses based on a switching spectroscopy strategy. The permanent phase transformation results in nonlinear diffracted intensity–voltage hysteresis loops. The excellent coincidence of the transformation threshold voltage with the coercive voltage of the titled polymorphic phase (S-BFO) clearly indicates that ferroelectric polarization switching in the S-BFO triggers the permanent phase transformation. The transient phase transition shows reversible changes in diffracted intensities under the application of an electric field. The lateral width of the tilted phases in real space is inversely proportional to the *in-plane* peak position in reciprocal space, indicating the motion of the phase boundary between multiple phases during the application of an electric field. In contrast, a real space mapping by *ex situ* x-ray nanodiffraction reveals that the permanent phase transformation occurs via the formation of the other phases.

II. EXPERIMENTAL DETAILS

The BiFeO₃ (BFO) thin film with a conducting bottom electrode of Pr_{0.5}Ca_{0.5}MnO₃ (PCMO) was grown on a (001) LaAlO₃ substrate by pulsed laser deposition with a KrF excimer laser

($\lambda = 248$ nm) operating at laser repetition rates of 10 Hz and 5 Hz for BFO and PCMO, respectively. The LAO substrate provides an in-plane compressive misfit strain of 0.3% for the epitaxial PCMO electrode layer. 50-nm thick Pt top electrodes with a diameter of 60 μ m were deposited on the BFO film by e-beam evaporator. X rays with a photon energy of 8 keV were focused on a spot of size 3 μ m using a Fresnel zone plate at the 9C beamline of the Pohang Accelerator Laboratory (PAL). Diffracted x rays from the sample were acquired using a gated pixel array detector (Pilatus 100K, Dectris Ltd.). A delay generator (DG 645, Stanford Research System, Ltd.) was used to generate reference signals in order to gate the detector and the electric pulses during acquisition. *Ex situ* x-ray nanodiffraction was conducted at the European Synchrotron Radiation Facility (ESRF). A monochromatic x ray with 8 keV was focused to a spot with a 100 nm full width at half maximum (FWHM) diameter using a Fresnel zone plate.

III. RESULTS AND DISCUSSION

The high compressive misfit strain of -4.5% between the BFO film and the LaAlO₃ (LAO) substrate leads to a coexistence of multiple crystallographic phases consisting of nanoscale stripe regions with alternation of the tilted T (T_{tilt}-BFO) and polymorphic (S-BFO) phases, and a surrounding tetragonal-like phase (T-BFO).¹⁷ A 50 nm-thick BFO film was grown on a Pr_{0.5}Ca_{0.5}MnO₃ (PCMO) bottom electrode/LAO substrate using the pulsed laser deposition technique.¹⁸ Figure 1(a) shows the distinct reflections near $Q_Z = 2.68 \text{ \AA}^{-1}$ at $Q_X = \pm 0.076 \text{ \AA}^{-1}$ and $Q_Z = 3.08 \text{ \AA}^{-1}$ at $Q_X = \pm 0.15 \text{ \AA}^{-1}$ in addition to a reflection at $Q_Z = 2.70 \text{ \AA}^{-1}$ and $Q_X = 0$, where Q_X and Q_Z are *in-plane* and *out-of-plane* scattering vectors, corresponding to S-, T_{tilt}-, and T-BFO at (002) Bragg reflection, respectively. The non-zero Q_X values of T_{tilt}- and S-BFO reflections indicate their tilted crystallographic orientation from the surface normal direction, while T-BFO possesses the same orientation with respect to the substrate.¹⁹ The distance of the peak of reflection from the origin of reciprocal space gives the c-lattice parameter of 4.07 \AA , 4.68 \AA , and 4.65 \AA for S-, T_{tilt}-, and T-BFO phases, respectively. The electric field-induced phase transformation in BFO thin films has been investigated using an *in situ* X μ D, as illustrated in Fig. 1(b). The focused x-ray beam size was 3 μ m in full width at half maximum (FWHM), which is sufficiently small to be located on a top electrode of the BFO film.

In order to investigate the relationship between the magnitude of the electric field and the dynamics for both phase transformations, we employed a switching spectroscopy setup based on a hysteresis loop type measurement with pulse sequences, as shown in Fig. 1(c).^{20,21} The diffraction patterns for the T, T_{tilt}, and S phases were accumulated using a 2D array detector while applying 5000 electric pulses with a duration of 30 μ s at the same amplitude as the capacitor. We defined the time intervals for the detection, 5 μ s at the beginning of a pulse and 100 μ s at the end of a pulse, as the on-field and off-field states, respectively, to avoid any effects arising from the charging and discharging time constants of the BFO capacitor. Figure 1(d) shows the diffraction patterns of the T phase with the amplitude of the applied voltage in the range of -9 V to $+9$ V.

The phase transformation has a direct impact on the diffracted intensities of T-, S-, and T_{tilt}-BFO at both the on- and off-field states,

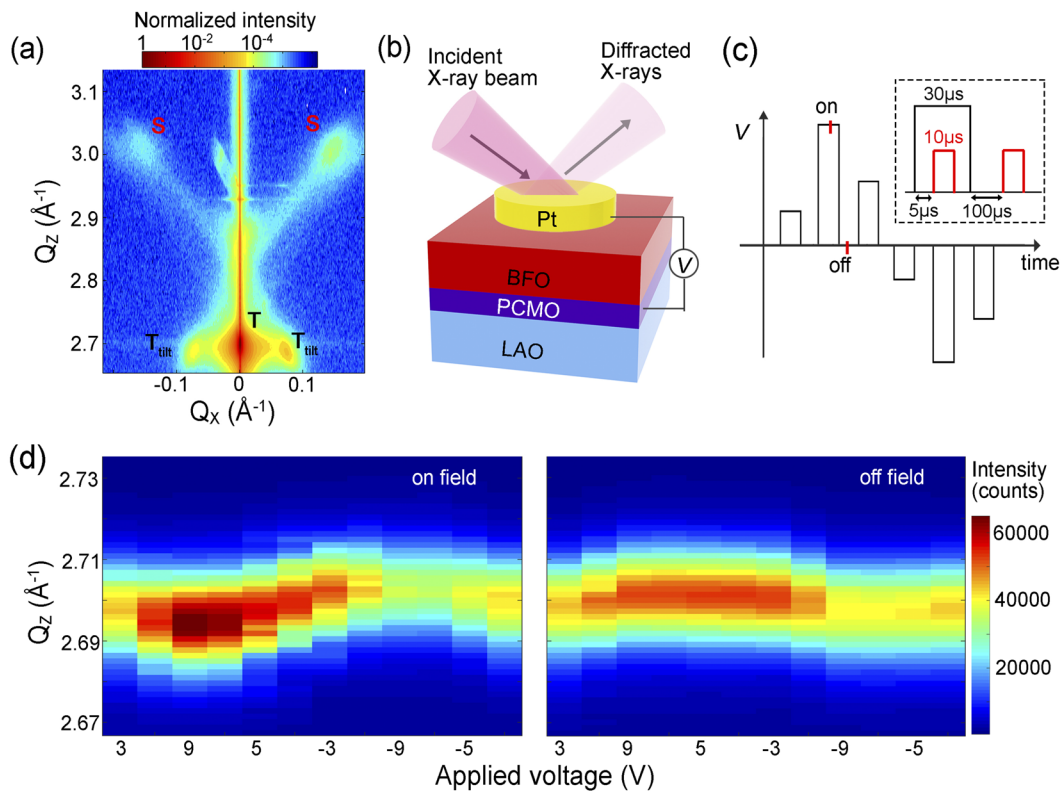


FIG. 1. (a) Reciprocal space maps (RSMs) of diffracted intensity as functions of Q_x and Q_z near (002) reflections from tetragonal (T), tilted polymorphic (S), and tilted T (T_{tilt}) phases in the 50-nm-thick BiFeO_3 thin-film capacitor. (b) Schematic illustration of the *in situ* x-ray microdiffraction ($X\mu\text{D}$) experiment with the application of electric fields. (c) Schematic diagram of the applied wave form during *in situ* $X\mu\text{D}$. The red lines inside and outside the pulse indicate the detection points for on- and off-field states, respectively. (d) Q_z -voltage map around T-BFO (002) Bragg reflection at $Q_x = 0$ at the (left) on-field and (right) off-field states.

as shown in Figs. 2(a)–2(c), respectively. We integrated the intensities along the Q_x direction and then extracted the peak positions using a Gaussian distribution function fit along the Q_z direction. The integrated intensity was normalized to an integrated intensity at the off-field state at $V = +3$ V. The diffracted intensities from three reflections at the off-field state show the hysteresis loops as a function of the magnitude of the electric field, owing to the permanent phase transformation. The diffracted intensity of T-BFO at the off-field state exhibits a conventional intensity–voltage hysteresis loop, i.e., an increase in the intensity with respect to the magnitude of the electric field, while both T_{tilt} and S-BFO show an opposite intensity–voltage hysteresis loop. After the application of a +9 V pulse, the integrated intensity of T-BFO increased by 20% compared with the initial intensity obtained after the application of a +3 V pulse. The opposite direction of the intensity–voltage hysteresis loops of the tilted phases indicates that the application of a positive voltage above +3 V induces a phase transformation from T_{tilt} - and S-BFO to T-BFO, and the application of a negative voltage below –3 V induces a phase transformation in the reverse direction.

We found that a ferroelectric polarization switching of S-BFO at the threshold voltage can trigger the permanent phase transformation, as shown in Fig. 2(d). The *out-of-plane* strain of T- and S-BFO

as a function of the magnitude of the applied voltage can provide clear information on polarization switching. The piezoelectric distortion results in lattice expansion parallel to the direction of electric field. The strain values were measured from the difference between the peak positions at the on- and off-field states. T-BFO exhibits a linear increase in the strain with increasing the amplitude of voltage. When the application of 9 V with the thickness of 50 nm gives the applied electric field (E) of 1.8 MV cm^{-1} , the measured longitudinal piezoelectric coefficient (d_{33}) is 11 pm V^{-1} , which is similar to experimentally reported and theoretically calculated d_{33} of T-BFO, indicating that the electric field was applied to the BFO film without huge loss. Using a thermodynamic model based on a Landau theory,²² a change in free energy of each phase under the electric field was calculated, giving -180 J cm^{-3} and -99 J cm^{-3} for T- and S-BFO at $E = 1.8 \text{ MV cm}^{-1}$, respectively. In contrast, S-BFO exhibits a butterfly-like loop, which is a classical ferroelectric switching behavior near the coercive voltage.^{21,23}

We speculate that the threshold voltage for the permanent phase transformation originates from the coercive voltage for ferroelectric polarization switching of S-BFO. Due to the higher coercive voltage of T-BFO than that of S-BFO,^{3,8} the application of voltage selectively induces ferroelectric polarization switching of S-BFO,

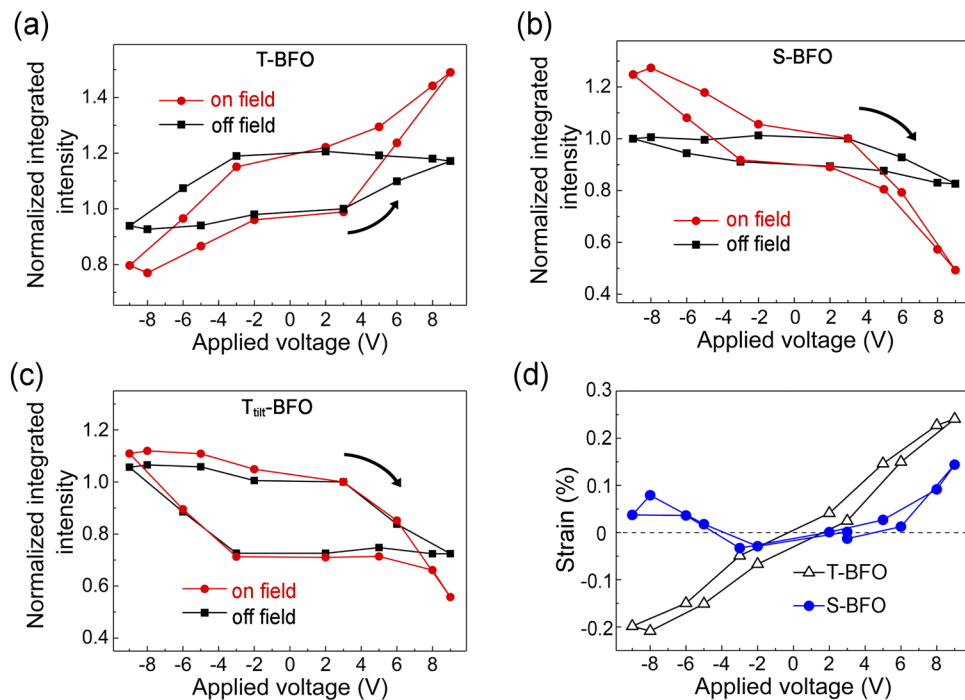


FIG. 2. Normalized integrated intensities as a function of amplitude of the applied voltage for (a) T-BFO, (b) S-BFO, and (c) T_{tilt} -BFO. The black and red lines represent the off and on-field states, respectively. The arrows in (a)–(c) denote the voltage sweep direction. (d) *Out-of-plane* strains of T-BFO (black triangles) and S-BFO (blue circles) as a function of amplitude of the applied voltage.

while T-BFO persists in the same direction as the ferroelectric polarization. We hypothesize that the permanent phase transformation did not occur without the polarization switching of S-BFO. We measured the phase transformation behavior of a 100 nm-thick BFO film grown on the PCMO/LAO substrate, as shown in Fig. S2 (see the [supplementary material](#)). The amplitude of the applied voltage ranged in ± 12 V. Under the application of the positive voltage, the intensity from T-BFO linearly increased with the decreasing intensity of S-BFO, which is a similar behavior of the transient phase transition observed from the 50-nm-thick BFO film. After turning off the voltage, both intensities of T- and S-BFO returned to the initial value, indicating that the electric field did not lead to the permanent phase transformation in a thicker BFO film. In contrast to the result of the 50-nm-thick BFO film, both T- and S-BFO exhibit a linear piezoelectric expansion without a change in sign, indicating that the direction of spontaneous polarization in both T- and S-BFO did not change. The absence of intensity hysteresis loop and switching behavior of S-BFO, together, consequently suggested that the permanent phase transformation is not available without the switching of S-BFO, while the transient phase transformation still occurs regardless of the film thickness.

In comparison to the permanent phase transformation, the transient phase transformation during the application of an electric field produced a higher slope in the diffracted intensity–voltage curve in the positive bias direction, as marked by the red lines in [Figs. 2\(a\)–2\(c\)](#). At +9 V, the normalized intensity of T-BFO,

T_{tilt} -BFO, and S-BFO is 1.49, 0.56, and 0.49, respectively, indicating an increase in the volume fraction of T-BFO and a decrease in that of the tilted phases. Conversely, at -9 V, the normalized intensity of T-BFO, T_{tilt} -BFO, and S-BFO is 0.80, 1.11, and 1.25, respectively, indicating a transformation from T-BFO to the tilted phases. According to the recent DFT calculations,⁹ the lower energy barrier between T- and S-BFO leads to sufficient piezoelectric lattice distortion to induce a phase transformation. Our calculations also showed that lattice expansion under a positive voltage energetically favors a phase transformation toward the T phase (see [Fig. S3 of the supplementary material](#)). The polarity-dependent electromechanical response due to the polarization switching of S-BFO can result in an asymmetric intensity, linked to the transformed volume fraction, as a function of voltage.

In order to understand the phase transformation at the nanoscale at both the off- and on-field states, we reconstructed the voltage-dependent three-dimensional reciprocal space by taking the reciprocal space map (RSM) obtained using a 2D x-ray detector. As shown in [Figs. 3\(a\) and 3\(b\)](#), the diffraction patterns at $Q_z = 2.68 \text{ \AA}^{-1}$ along the *in-plane* scattering vector Q_x indicate that the transient phase transformation at the on-field state is associated with the *in-plane* peak position of T_{tilt} -BFO reflections. In contrast, the permanent phase transformation at the off-field state shows changes in intensity without a shift of the *in-plane* peak position. We hypothesize that the nanoscale phase evolution for the permanent phase transformation at the off-field state is physically

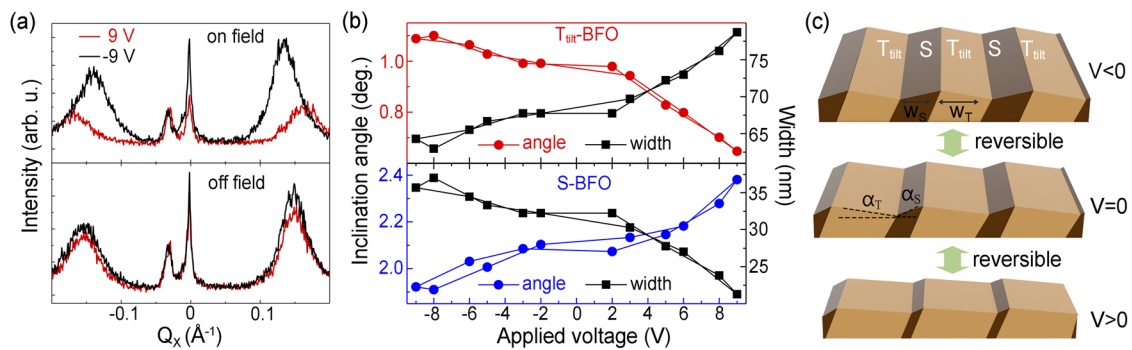


FIG. 3. (a) X-ray diffraction profiles of $T_{\text{tilt}}\text{-BFO}$ at $Q_z = 2.68 \text{ \AA}^{-1}$ along the Q_x direction at (top) on-field and (bottom) off-field states. (b) Averaged inclination angle estimated from the *in-plane* peak positions of the T_{tilt} phase under an applied electric field. (c) Schemes for the complex phase boundary motion for the transient phase transformation mechanism under positive bias (bottom) and negative bias (top) from the initial state (middle).

different from that for the transient phase transformation at the on-field state.

The inclination angles converted from the Q_x peak position for $T_{\text{tilt}}\text{-BFO}$ and S-BFO at the on-field state were analyzed, as shown in Fig. 3(c). The absolute value of the inclination angle of $T_{\text{tilt}}\text{-BFO}$ gradually decreases with an increase in the magnitude of V_{film} , while the S-BFO reflection exhibits a decrease in the inclination angle under the positive voltage. The angle of $T_{\text{tilt}}\text{-BFO}$ decreased from 0.93° to 0.63° , and that of S-BFO increased from 2.15° to 2.38° . When a mean lateral width of the phase (W_L) is inversely proportional to the inclination angle,^{24,25} the inclination angle dependence of the width of $T_{\text{tilt}}\text{-}$ and S-BFO can be evaluated quantitatively. The ratio of the width of these phases (W_T/W_S) can be defined as $\sin(\alpha_S)/\sin(\alpha_T)$, where W_T , W_S , α_T , and α_S are the width of $T_{\text{tilt}}\text{-BFO}$, width of S-BFO, inclination angles of $T_{\text{tilt}}\text{-BFO}$, and S-BFO, respectively. The evaluated W_T/W_S at +3 V, as the initial state, which is 2.3, is similar to the reported ratio of the lateral widths.¹⁸ The ratio, W_T/W_S , at +9 V and -9 V is 3.8 and 1.73, respectively, indicating

that the phase transformation between the tilted phases occurs during a transient phase transformation, as shown in Fig. 3(c). When the sum of W_T and W_S is $\sim 100 \text{ nm}$ at the initial state,^{18,26} W_T under +9 V and -9 V becomes 79 nm and 63 nm, respectively.

Although a variation of the lateral width appears during the transient phase transformation, this model does not, *per se*, clarify the transformation between the tilted phases and T-BFO. In order to take into account a nanoscale transformation between the tilted phases and T-BFO for a transient transformation, this should also involve transitions among the tilted phases and T-BFO,²⁷ which is not quite matching with the previously proposed model involving a sequential phase transformation,¹⁰ as shown in Fig. 3(c). At the positive bias, the model for the complex motion of the phase boundary shows that an increase in width of $T_{\text{tilt}}\text{-BFO}$ and a decrease in the width of S-BFO occurs simultaneously, with a reduction of both the tilted phases along the vertical width perpendicular to the lateral width. When the diffracted intensity is proportional to the volume of the phase, corresponding to the product of vertical and lateral

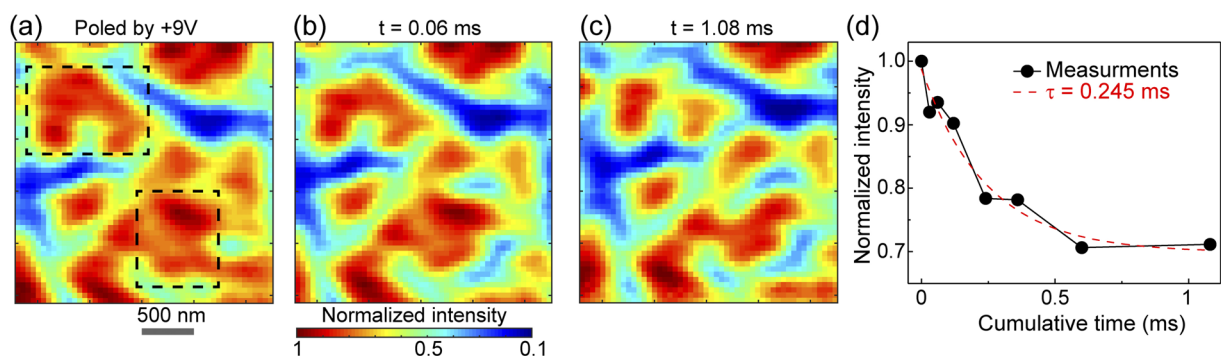


FIG. 4. Real space maps of x-ray reflection from T-BFO phases (a) after poling under +9 V, (b) after applying two electric pulses, and (c) applying 30 electric pulses with an amplitude of -9 V and a duration of $30 \mu\text{s}$. The cumulative time of application of -9 V for (b) and (c) is 0.06 ms and 1.08 ms, respectively. A scheme for the sequence of the applied electric voltage during real space mapping is provided in Fig. S5b of the [supplementary material](#). (d) Normalized integrated intensity of the whole areas of (a)–(c) as a function of cumulative time. The dashed lines are the fit results of an exponential decay function.

widths, the voltage dependent vertical width can be estimated as shown in Fig. S4.

The nanoscale aspect of the permanent phase transformation has been investigated by mapping the diffracted intensity in real space using *ex situ* x-ray nanodiffraction, beamline ID01 at the ESRF.²⁸ As shown in Fig. S5, we first applied the positive voltage to induce a permanent phase transformation from the tilted phases to T-BFO. Then, we measured the real-space mapping of x-ray reflection of T-BFO after applying various numbers of the electric pulse with a duration of 30 μ s. Figure 4(a) shows the real space map of the diffracted intensity from T-BFO reflection after the application of the positive bias. The contrast intensity of the T-BFO reflection in the real space map arises from the coexisting morphology T-BFO and the tilted phases. Then, we applied a few negative pulses with a duration of 30 μ s. Figures 4(b) and 4(c) show the real space map after application of 2 and 36 pulses corresponding to a cumulative time of 30 μ s and 1080 μ s, respectively. The decrease in intensity of T-BFO is apparent in specific regions marked by boxes in Fig. 4(a), indicating that the permanent phase transformation occurs

via the nucleation of phases rather than the motion of the phase boundary.

The dynamics of the permanent phase transformation was analyzed by monitoring the diffracted intensity from the T-BFO reflection as a function of the cumulative time, as shown in Fig. 4(d). We integrated the intensities corresponding to the measured area and plotted the intensity as a function of the cumulative time. Using an exponential decay function, we found that the time constant for the fitted result is 0.245 ms. The ferroelectric polarization switching of S-BFO can be attributed to the slow transformation time dynamics in the μ s regime. Note that the general switching time of ferroelectric polarization in similar thin-film capacitor structures has been reported to be longer than a few tens of μ s.²⁹ This strongly suggests that selective switching of S-BFO in the restricting condition of being surrounded by the other phases with an opposite polarization direction would require a higher electric field or a longer switching time.³⁰ The nanoscale mechanisms of the permanent and transient phase transformation process are illustrated in Fig. 5.

IV. CONCLUSION

We investigated the voltage-dependent evolution dynamics of multiple crystalline phases in the highly strained BFO film using *in situ* X μ D. We found that selective switching is the main factor in determining the threshold field of a permanent transformation (± 3 V for the 50-nm-thick film). The complex motion of the phase boundary for the transient phase transformation during the application of an electric field has been visualized, which allows us to manipulate the functionalities of nanoscale devices. We propose that our findings will stimulate further theoretical studies and syntheses for the engineering of electrostatic energy of multiple crystalline phases. The nanosecond phase transformations driven by an applied electric field in multiferroic BFO would significantly impact the design of multiferroic based high-speed electronic devices.

SUPPLEMENTARY MATERIAL

See the [supplementary material](#) for the voltage dependent RSMs of mixed phases, thickness dependent intensity loops, DFT calculation, and the detailed information of nanodiffraction.

AUTHORS' CONTRIBUTIONS

H.J.L. and J.Y.J. designed the experiments. J.K. and C.-H.Y. synthesized epitaxial BiFeO₃ thin films. H.J.L., S.H.H., and S.Y.L. carried out the *in situ* x-ray microdiffraction at the PAL. H.J.L., S.H.H., H.C., S.G., T.S., C.R., U.P., and J.Y.J. carried out the *ex situ* x-ray nanodiffraction at the ESRF. Y.-J.H., P.-E.J., I.K., J.-H.L., and J.Y.J. calculated density functional theory. H.J.L. and J.Y.J. analyzed data and wrote the manuscript. J.Y.J. supervised the research. All authors contributed to the discussions and manuscript preparation.

ACKNOWLEDGMENTS

J.Y.J. acknowledges support from the National Research Foundation of Korea (NRF) funded by the Korean Government

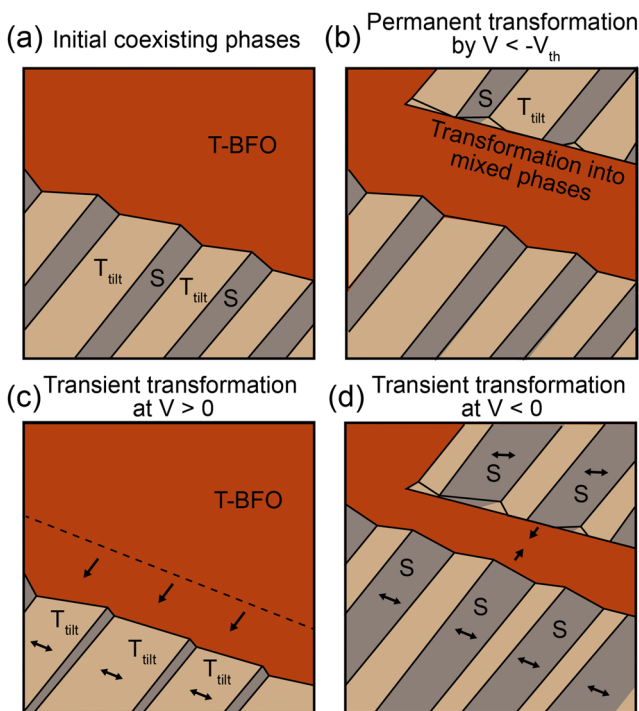


FIG. 5. (a) Initial microstructure consisting of pure T-BFO and mixed stripe regions with alternation of the T_{tilt} -BFO and S-BFO. (b) Permanent phase transformation occurred via the generation of the region of mixed phases when the applied voltage is smaller than the negative threshold voltage ($-V_{\text{th}}$). (c) Transient phase transformation available only during the application of the positive voltage to the structure in (a), involving the expansion of T-BFO into the region of mixed phases and transformation from S-BFO to T_{tilt} -BFO. (d) Transient phase transformation with a reduction in T-BFO and transformation from T_{tilt} -BFO to S-BFO during the application of the negative voltage to the structure in (b). The arrows in (c) and (d) indicate the direction of phase boundary movements during transient phase transformation.

(Grant Nos. 2020R1A2C200612711, 2020K1A3A7A09080404, and 2017M3D1A1040828), MSIP and PAL, the GRI (GIST Research Institute) project by GIST, and the National Strategic Project-Fine particle of the National Research Foundation of Korea (NRF) supported by the Ministry of Science and ICT (MSIT), the Ministry of Environment (ME), and the Ministry of Health and Welfare (MOHW) (Grant No. 2017M3D8A1091937). H.J.L. acknowledges support from the NRF (Grant No. 2017R1A6A3A11030959). C.-H.Y. acknowledges support from the NRF grant via the Creative Research Initiative Center for Lattice Defectronics (Grant No. 2017R1A3B1023686).

DATA AVAILABILITY

The data that support the findings of this study are available within the article and its [supplementary material](#), or from the corresponding author upon reasonable request.

REFERENCES

- R. J. Zeches, M. D. Rossell, J. X. Zhang, A. J. Hatt, Q. He, C.-H. Yang, A. Kumar, C. H. Wang, A. Melville, C. Adamo, G. Sheng, Y.-H. Chu, J. F. Ihlefeld, R. Erni, C. Ederer, V. Gopalan, L. Q. Chen, D. G. Schlom, N. A. Spaldin, L. W. Martin, and R. Ramesh, *Science* **326**, 977 (2009).
- K.-T. Ko, M. H. Jung, Q. He, J. H. Lee, C. S. Woo, K. Chu, J. Seidel, B.-G. Jeon, Y. S. Oh, K. H. Kim, W.-I. Liang, H.-J. Chen, Y.-H. Chu, Y. H. Jeong, R. Ramesh, J.-H. Park, and C.-H. Yang, *Nat. Commun.* **2**, 567 (2011).
- J. X. Zhang, Q. He, M. Trassin, W. Luo, D. Yi, M. D. Rossell, P. Yu, L. You, C. H. Wang, C. Y. Kuo, J. T. Heron, Z. Hu, R. J. Zeches, H. J. Lin, A. Tanaka, C. T. Chen, L. H. Tjeng, Y. H. Chu, and R. Ramesh, *Phys. Rev. Lett.* **107**, 147602 (2011).
- L. You, P. Caesario, L. Fang, P. Ren, L. Wang, Y. Zhou, A. Gruverman, and J. Wang, *Phys. Rev. B* **90**, 134110 (2014).
- D. Sando, Y. Yang, E. Bousquet, C. Carrétéro, V. Garcia, S. Fusil, D. Dolfi, A. Barthélémy, P. Ghosez, L. Bellaiche, and M. Bibes, *Nat. Commun.* **7**, 10718 (2016).
- A. Herklotz, S. F. Rus, N. Balke, C. Rouleau, E.-J. Guo, A. Huon, S. Kc, R. Roth, X. Yang, C. Vaswani, J. Wang, P. P. Orth, M. S. Scheurer, and T. Z. Ward, *Nano Lett.* **19**, 1033–1038 (2019).
- D. Sando, B. Xu, L. Bellaiche, and V. Nagarajan, *Appl. Phys. Rev.* **3**, 011106 (2016).
- J. X. Zhang, B. Xiang, Q. He, J. Seidel, R. J. Zeches, P. Yu, S. Y. Yang, C. H. Wang, Y.-H. Chu, L. W. Martin, A. M. Minor, and R. Ramesh, *Nat. Nanotechnol.* **6**, 98–102 (2011).
- M. P. Cosgriff, P. Chen, S. S. Lee, H. J. Lee, L. Kuna, K. C. Pitike, L. Louis, W. D. Parker, H. Tajiri, S. M. Nakhmanson, J. Y. Jo, Z. Chen, L. Chen, and P. G. Evans, *Adv. Eletron. Mater.* **2**, 1500204 (2016).
- A. R. Damodaran, C.-W. Liang, Q. He, C.-Y. Peng, L. Chang, Y.-H. Chu, and L. W. Martin, *Adv. Mater.* **23**, 3170–3175 (2011).
- A. B. Naden, D. Edwards, S. M. Neumayer, J. G. M. Guy, B. J. Rodriguez, N. Bassiri-Gharb, and A. Kumar, *Adv. Mater. Interfaces* **5**, 1801019 (2018).
- D. Edwards, N. Browne, K. M. Holsgrove, A. B. Naden, S. O. Sayedghae, B. Xu, S. Prosandeev, D. Wang, D. Mazumdar, M. Duchamp, A. Gupta, S. V. Kalinin, M. Arredondo, R. G. P. McQuaid, L. Bellaiche, J. M. Gregg, and A. Kumar, *Nanoscale* **10**, 17629–17637 (2018).
- Z. Chen, Z. Luo, C. Huang, Y. Qi, P. Yang, L. You, C. Hu, T. Wu, J. Wang, C. Gao, T. Sritharan, and L. Chen, *Adv. Funct. Mater.* **21**, 133–138 (2011).
- O. Diéguez, O. E. González-Vázquez, J. C. Wojdeł, and J. Íñiguez, *Phys. Rev. B* **83**, 094105 (2011).
- R. K. Vasudevan, Y. Liu, J. Li, W.-I. Liang, A. Kumar, S. Jesse, Y.-C. Chen, Y.-H. Chu, V. Nagarajan, and S. V. Kalinin, *Nano Lett.* **11**, 3346–3354 (2011).
- P. Sharma, Y. Heo, B. K. Jang, Y. Y. Liu, J. Y. Li, C. H. Yang, and J. Seidel, *Sci. Rep.* **6**, 32347 (2016).
- C. Beekman, W. Siemons, T. Z. Ward, M. Chi, J. Howe, M. D. Biegalski, N. Balke, P. Maksymovych, A. K. Farrar, J. B. Romero, P. Gao, X. Q. Pan, D. A. Tenne, and H. M. Christen, *Adv. Mater.* **25**, 5561–5567 (2013).
- K. Chu, B.-K. Jang, J. H. Sung, Y. A. Shin, E.-S. Lee, K. Song, J. H. Lee, C.-S. Woo, S. J. Kim, S.-Y. Choi, T. Y. Koo, Y.-H. Kim, S.-H. Oh, M.-H. Jo, and C.-H. Yang, *Nat. Nanotechnol.* **10**, 972 (2015).
- Z. L. Luo, H. Huang, H. Zhou, Z. H. Chen, Y. Yang, L. Wu, C. Zhu, H. Wang, M. Yang, S. Hu, H. Wen, X. Zhang, Z. Zhang, L. Chen, D. D. Fong, and C. Gao, *Appl. Phys. Lett.* **104**, 182901 (2014).
- S. Jesse, A. P. Baddorf, and S. V. Kalinin, *Appl. Phys. Lett.* **88**, 062908 (2006).
- H. J. Lee, E.-J. Guo, T. Min, S. H. Hwang, S. Y. Lee, K. Dörr, J. Lee, and J. Y. Jo, *Nano Res.* **11**, 3824–3832 (2018).
- V. G. Koukhar, N. A. Pertsev, and R. Waser, *Phys. Rev. B* **64**, 214103 (2001).
- A. Grigoriev, R. J. Sichel, J. Y. Jo, S. Choudhury, L.-Q. Chen, H. N. Lee, E. C. Landahl, B. W. Adams, E. M. Dufresne, and P. G. Evans, *Phys. Rev. B* **80**, 014110 (2009).
- S. Utsugi, T. Fujisawa, R. Ikariyama, S. Yasui, H. Nakaki, T. Yamada, M. Ishikawa, M. Matsushima, H. Morioka, and H. Funakubo, *Appl. Phys. Lett.* **94**, 052906 (2009).
- H. J. Lee, T. Shimizu, H. Funakubo, Y. Imai, O. Sakata, S. H. Hwang, T. Y. Kim, C. Yoon, C. Dai, L. Q. Chen, S. Y. Lee, and J. Y. Jo, *Phys. Rev. Lett.* **123**, 217601 (2019).
- L. You, Z. Chen, X. Zou, H. Ding, W. Chen, L. Chen, G. Yuan, and J. Wang, *ACS Nano* **6**, 5388–5394 (2012).
- Y. Ahn, A. Pateras, S. D. Marks, H. Xu, T. Zhou, Z. Luo, Z. Chen, L. Chen, X. Zhang, A. D. DiChiara, H. Wen, and P. G. Evans, *Phys. Rev. Lett.* **123**, 045703 (2019).
- S. J. Leake, G. A. Chahine, H. Djazouli, T. Zhou, C. Richter, J. Hilhorst, L. Petit, M.-I. Richard, C. Morawe, R. Barrett, L. Zhang, R. A. Homs-Regojo, V. Favre-Nicolin, P. Boesecke, and T. U. Schüllli, *J. Synchrotron Radiat.* **26**, 571–584 (2019).
- E. J. Guo, K. Dörr, and A. Herklotz, *Appl. Phys. Lett.* **101**, 242908 (2012).
- J. Y. Jo, P. Chen, R. J. Sichel, S. J. Callori, J. Sinsheimer, E. M. Dufresne, M. Dawber, and P. G. Evans, *Phys. Rev. Lett.* **107**, 055501 (2011).